Naples, 11/10/2018

Dear referee,

Thanks for your comments, which we have carefully taken into account.

We tried to improve the figure captions according to your suggestions.

We thank you very much for your consideration and we send you our best regards.

On behalf of the authors
Dr. Diana Di Luccio
Dr. Luigi Mucerino

Wave run-up prediction and observation in a micro-tidal beach

Diana Di Luccio[1], Guido Benassai[2], Giorgio Budillon[1], Luigi Mucerino[3], Raffaele Montella[1], and
Eugenio Pugliese Carratelli[4]

[1]University of Naples "Parthenope", Science and Technologies Department, Centro Direzionale Is. C4, 80143 Napoli, Italy
[2]University of Naples "Parthenope", Engineering Department, Centro Direzionale Is. C4, 80143 Napoli, Italy
[3]University of Genova, Department of Earth, Environment and Life Sciences, Corso Europa 26, 16132 Genova, Italy
[4]Inter-University Consortium for the Prediction and Prevention of Major Risks Hazards (CUGRI), 84080 Penta di Fisciano
(SA), Italy

Correspondence to: Diana Di Luccio (diana.diluccio@uniparthenope.it)

Abstract. Extreme weather events bear a significant impact on coastal human activities and on the related economy. Forecasting
and hindcasting the action of sea storms on piers, coastal structures and beaches is an important tool to mitigate their effects.
To this end, with particular regard to low coasts and beaches, the Authors have developed a computational model chain based
partly on open access models and partly on an ad-hoc developed numerical calculator to evaluate beach wave run-up levels
and flooding. The offshore wave simulations are carried out with a version of the WaveWatch III model, implemented by
CCMMMA (Campania Centre for Marine and Atmospheric Monitoring and Modelling - University of Naples "Parthenope"),
validated with remote sensing data. The waves thus computed are in turn used as initial conditions for the run-up calculations,
carried out with various empirical formulations; the results were finally validated by a set of specially conceived video camera-
based experiments on a micro-tidal beach located on the Ligurian Sea. Statistical parameters are provided on the agreement
between the computed and observed values. It appears that, while the system is a useful tool to properly simulate the beach
flooding during a storm, empirical run-up formulas, when used in coastal vulnerability context, have to be carefully chosen,
applied and managed particularly on gravel beaches.

Keywords: model chain, wave numerical model, beach run-up, video monitoring.

1 Introduction

Real time forecast and hindcast systems for ocean and coastal risks are becoming more and more common; the availability of
both global and regional weather and sea state modelling systems has put the development of warning systems within reach of
local Authorities and Engineering Companies. Such systems, however, are generally aimed at providing real time evaluation of
damage on coastal infrastructure or dwellings rather than on risks of beach flooding. Assessing and forecasting such hazards is
an ever increasing concern, especially in areas where seaside tourism is an essential part of the economy, as for instance in most
Mediterranean countries. Although in recent years a large number of papers have been published on the validation of offshore
numerical models, to the best of our knowledge very few studies have been published on the development and the application
of operational models including the effects on the beaches; hence this paper is aimed at validating a whole chain of models to
simulate the action of waves, starting from wind and off-shore wave formation, through wave propagation down to the final
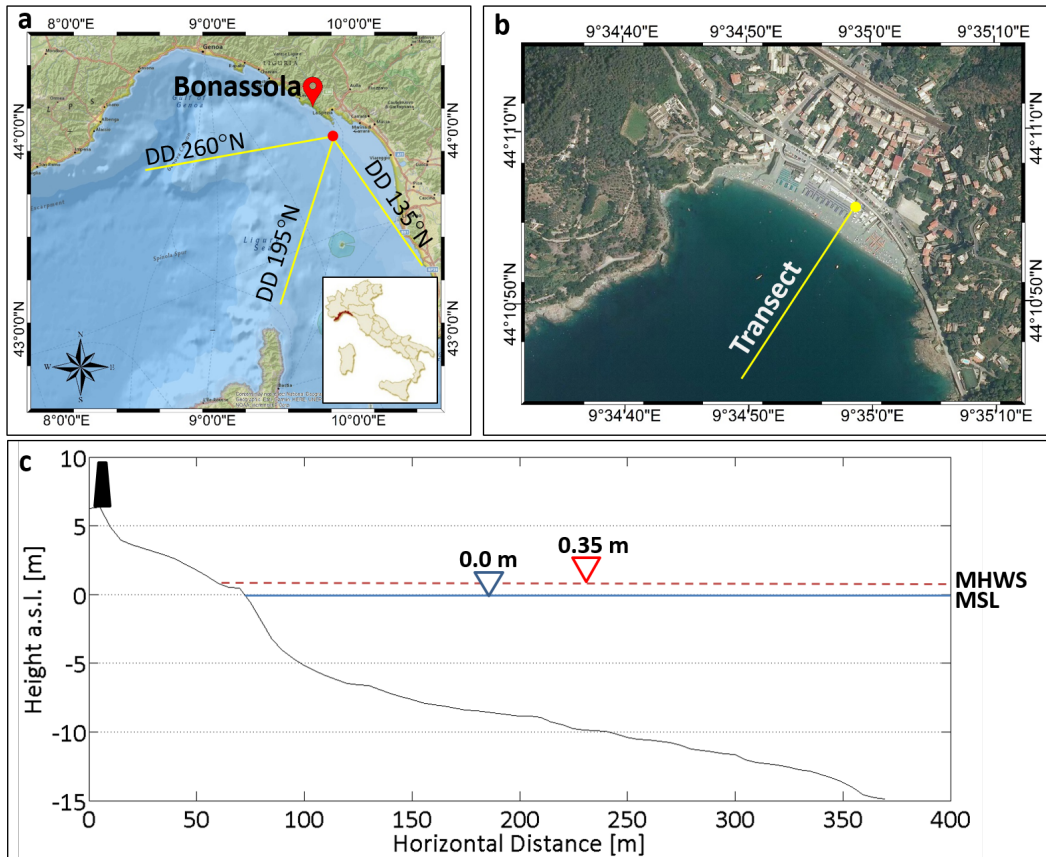
Figure 1. Bonassola beach study area with (a) the location of La Spezia SWAN buoy (red circle) and the main and secondary fetches (Image Source: National Geographic); (b) the monitored cross-shore transect with video-camera system location (yellow circle), (image source: http://www.pcn.minambiente.it/mattm/servizio-wms/); (c) the beach profile along the transect with the location of the anthropic structures (black trapezium), mean sea level (MSL) and the mean spring tidal range (MHSW) were extracted by the official Italian tide archives(http://www.mereografico.it)

.

segment, which involves the analysis of set-up and run-up on the coast. In particular, a specially conceived experimental set-up has been prepared on the final stage, i.e. flooding of the beach. In the following, the state of art of each component of the model chain will be very briefly discussed, while some more detail will be provided on the wave run-up and beach flooding and on the related experimental techniques.

5 The computation of winds and offshore waves is a well settled field, both from the point of view of the research and of the operational procedure (Bertotti and Cavaleri, 2009; Cavaleri and Rizzoli, 1981; Mentaschi et al., 2013; Benassai and Ascione, 2006a). Also the assimilation of wave measurements is a well tested technique (see for instance Bidlot et al. (2002)).

The monitoring and forecasting of wind-wave interaction processes is however particularly critical along coastal areas, which are highly dynamic complex systems that respond in a nonlinear manner to external perturbations: for instance coastal vulner-

10 ability has been considered by many researchers (Didenkulova, 2010; Di Paola et al., 2014; Di Luccio et al., 2018), also taking into account sea-level rise (Benassai et al., 2015a) and subsidence (Aucelli et al., 2016). Measurements are often difficult: satellite data do not reach the adequate resolution and quality when approaching the coast (Aulicino et al., 2018; Cotroneo et al., 2016). The quality of predicted wave data depends on the quality of driving wind fields (Rusu et al., 2014), which are normally provided by global forecasting models, satellite altimeters (Benassai et al., 2015b; Reale et al., 2018), or alternatively

15 by satellite-based microwave Synthetic Aperture Radar (SAR) (Johannessen and Bjorgo, 2000). Much work has been done on the reliability of these data sources and their application is now common practice (Benassai et al., 2013a, b, 2018; Dentale et al., 2018).

We focused our attention the wave run-up prediction, wave run-up prediction is required in most coastal vulnerability and risk evaluation projects (Didenkulova and Pelinovsky, 2008; Didenkulova et al., 2010). Wave run-up Ru is defined as "the landward

20 extent of wave uprush measured vertically from the still water level" (Melby et al., 2012). Although complex numerical models are required (Dodd, 1998; Hubbard and Dodd, 2002) to provide accurate estimates of wave run-up with given boundary conditions, simplified run-up formulas are useful to give realistic results on existing cross-shore profiles. The earliest formulation of run-up height was provided in Hunt (1959) who calculated run-up from incident regular waves. He provided the following equation (here, as in most empirical formulas, Ru includes the wave set-up)

25
$$\frac{Ru}{H_0} = \xi \tag{1}$$

where ξ is the Iribarren number or surf similarity parameter (Battjes, 1975)

$$\xi = \frac{tan\beta}{\sqrt{\frac{H_0}{L_0}}} \tag{2}$$

and β is the beach slope angle, H_0 is the deep water significant wave height and L_0 is the linear theory deep-water wavelength (Airy, 1841)

30
$$L_0 = \frac{gT^2}{2\pi} \tag{3}$$

and T is the wave period.

Holman (1986) measured extreme value statistics of wave run-up on a shoreline from a single beach and correlated them with

the offshore Irribarren number. Mase (1989) performed an extensive series of laboratory tests for the prediction of run-up elevations of random waves on gentle smooth and impermeable slopes as a function of surf similarity parameter. He included irregular waves and statistical values of the obtained run-up levels, that is Ru_{max} (the highest run-up elevation), $Ru_{2\%}$ (the run-up elevation which is exceeded by 2%), $Ru_{10\%}$ (the run-up elevation which is exceeded by 10%), $Ru_{33\%}$ (the run-up elevation

5 which is exceeded by 33%), Ru_{mean} (the average of the total run-up elevation) (van der Meer et al., 2016). He also introduced two coefficients which are dependent on the characteristic run-up level.

Stockdon et al. (2006) extended the work of Holman (1986) to several beaches covering a wide range of offshore wave conditions to derive a parametric predictor of the total run-up height. They considered the run-up level $Ru_{2\%}$ as a function of the two different contributions of wave set-up and swash.

10 Poate et al. (2016) demonstrated that wave run-up on gravel beaches under energetic wave conditions was significantly under predicted by the Stockdon et al. (2006) equation and proposed a new run-up parametrization for (pure) gravel beaches. They made clear that on sandy beaches under extreme waves, run-up conditions becomes dominated by infragravity waves (Guza and Thornton, 1982; Senechal et al., 2011) with the incident storm waves breaking and dissipating their energy further offshore, whereas on gravel beaches very large waves can impact directly on the beach.

15 Video recording observations of run-up on a wide range of storm wave conditions was performed, among others, by Ruggiero et al. (2004) and Bryan and Coco (2007) who collected vertical run-up elevation time series using the "timestack" method (Aagaard and Holm, 1989; Holland and Holman, 1993). Since then, a number of run-up measurements using remote video imagery of the beaches have been carried out. Further work along this line was carried out by Stockdon et al. (2007), who calculated wave run-up elevation and setup from modeled offshore wave conditions using SWAN (Sea WAve

20 measurement Network) and an empirical parametrization (Stockdon et al., 2006) for the evaluation of coastal vulnerability and run-up elevation. In the last few years USGS National Assessment of Coastal Change Hazards project is working in collaboration with the National Oceanic and Atmospheric Administration (NOAA)/National Weather Service (NWS) and the National Center for Environmental Prediction (NCEP) to produce total water level and coastal change forecasts (https://coastal.er.usgs.gov/hurricanes/research/twlviewer/). This operational model combines NOAA wave and water level

25 predictions and a USGS wave run-up model with beach slope observations to provide regional weather offices with detailed forecasts of total water levels (Stockdon et al., 2012; Doran et al., 2015). Following Paprotny et al. (2014), forecasts of wave run-up on two beaches of Polish Baltic Sea coast were tested to evaluate flooding, by chaining WAM wave model with run-up empirical formulas, during SatBaltyk Operating System-Shores.

In this paper wave run-up levels were computed with the various different formulations described above. Since no local mea-

30 surements from buoys were available (Montella et al., 2008), a version of WaveWatch III (WW3) model was used, as implemented by the Campania Centre for Marine and Atmospheric Monitoring and Modelling (CCMMMA) - University of Naples "Parthenope", by making full use of a high spatial resolution weather-ocean forecasting system with a high performance computing (HPC) system for simulation and open environmental data dissemination (Montella et al., 2007). This deep-water numerical model (Ascione et al., 2006) was coupled with a wave propagation model in shallow water which provided the run-

35 up evaluation on the beach. This model chain was tested on a micro-tidal beach located on the Ligurian Sea, in order to assess

the reliability of the wave modelling system, already verified in offshore conditions by means of in-situ and remote sensing techniques (Carratelli et al., 2007; Reale et al., 2014; Benassai and Ascione, 2006b).

This paper is organized as follows: the field data and the numerical models are reported in Sections 2 and 3, the results and validation are given in Section 4. Lastly, our discussion and the conclusions are reported in Sections 5 and 6, respectively.

5 2   Study area and wave climate

The experiments presented in this paper were carried out on the Bonassola beach (La Spezia, Italy), which is approx. 410m long, and is located on the eastern coast of Liguria. The coastline is oriented South-East/North-West and it is exposed to waves coming from the South-West (215°-245°), while it is protected from the South-East waves. Bonassola beach can be classified as mixed gravel-sand (MSG) beach due to its sediment characteristics and its morphology (Jennings and Shulmeister (2002)). The range of mean sediment grain size in the swash zone is 0.76mm to 62.65mm (0.38 to -5.96 ϕ). The mean beach slope is approximately 8.3% from the shoreline to 10m water depth and becomes 5.5% between 10m and 30m (Fig. 1c). The offshore beach is made up of a mixture of mean and coarse sand. The data of the grain size and the slope of the beach were taken from a geomorphological survey conducted by the University of Genova in 2012 and reported in Balduzzi et al. (2014).
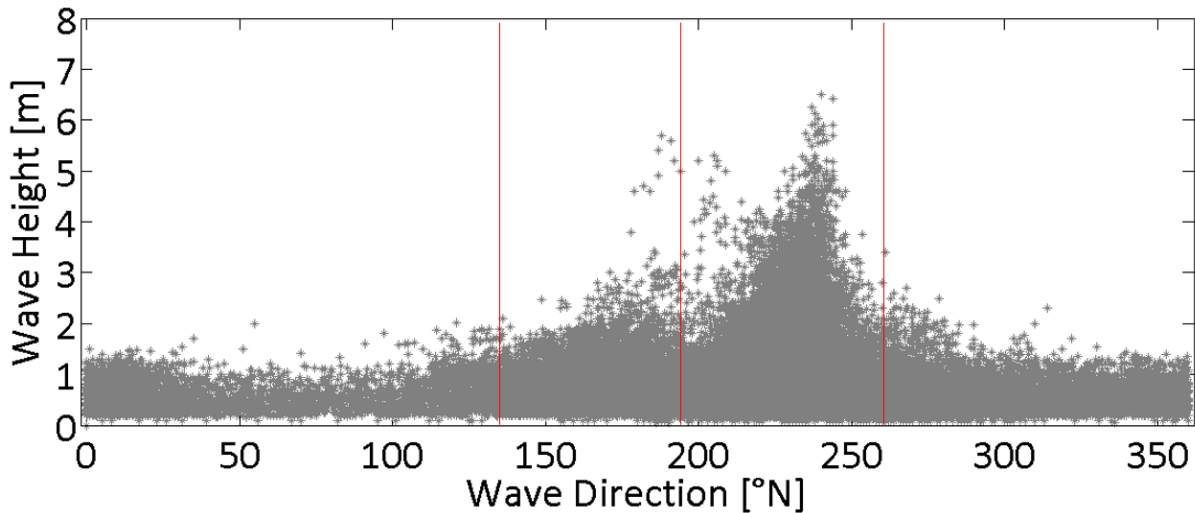
Figure 2. Significant wave heights and wave directions recorded from the SWAN buoy of La Spezia 1989-2009. Red lines marked the sectors of waves origin: 195°N-260°N (the main fetch) and 135°N-195°N (the secondary fetch).

The offshore wave climate was estimated by using the data recorded by the Italian RON (Italian National Wavemeter System) buoy located offshore La Spezia (43°55'41.99"N, 09°49'36.01"E) from 1989 to 2009. The main fetch sector is comprised between directions 195°N and 260°N while the secondary fetch is limited by the directions 135°N and 195°N (in the following S1). The main transverse sector was then subdivided into two sub-sectors, 195-225°N (S_2) and 225-260°N (S_3), in which two different wave conditions were observed: the maximum significant wave height (H_s) is lower than 5.5m between 195°N and
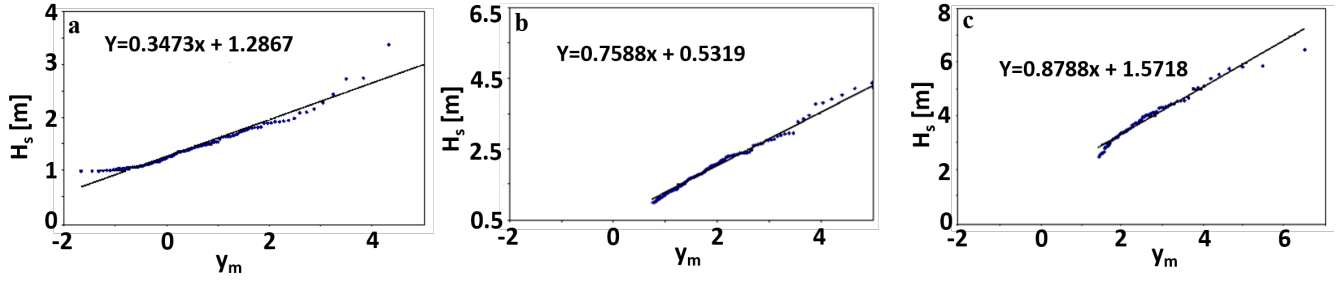
Figure 3. Matching between the recorded extreme wave heights and the reduced variable for Gumbel distribution function for waves coming from a) 135°N-195°N; b) 195°N-225°N; c) 225°N-260°N. <mark>The dataset is relative to the records of La Spezia wave buoy in the period 1989-2009.</mark>

225°N and higher than 5.5m between 225°N and 260°N (Fig. 2).

A representative sample of statistically independent extreme wave events N was selected on the basis of the Peak Over Threshold method (Goda, 1989). The 48h-maxima based on over-threshold H^* time series has been sorted in order to find the best fit between the data and the Gumbel (Fisher-Tippet I) cumulative probability distribution function.

$$5 \quad P(H) = e^{-e^{-\left(\frac{H-B}{A}\right)}} \tag{4}$$

where A is the location parameter and B is the scale parameter. A rank index m, ranging from 1 to N was associated to order the array and the sample rate of non-exceedance $F(H_s<H^*)$ was calculated as

$$F(H_s) < H^* = 1 - \frac{m - 0.44}{N + 0.12} \tag{5}$$

and it is assumed coincident with the non exceedance probability.

$$10 \quad y_m = -ln[-lnF(H_s < H^*)] \tag{6}$$

Figure 3 shows the rate between $H_s<H^*$ and relative reduced variable for waves coming from each directional sector.

The linear regression line $y=ax+b$ is given as

$$H_s = Ay_m + B \tag{7}$$

where A (slope of the regression line) and B (line intercept) coefficients are linked with the probability distribution function. The significant wave height H_r with return period T_r can be determined by the following expressions:

$$H_r = Ay_r + B \tag{8}$$

where the relative reduced variable is

$$y_r = -ln\left[-ln\left(1 - \frac{1}{\lambda T_r}\right)\right] \tag{9}$$

Table 1. Design waves, in terms of H_r associated to different return periods (T_r equal to 1, 5, 10, 20, 50 and 100 years), obtained from La Spezia buoy (1989-2009) for each directional sector (S_1, S_2 and S_3).

T_r [yr]	Sector	H_r [m]	y_r	T_r [yr]	Sector	H_r [m]	y_r
	S_1	2.84	4.46		S_1	3.88	7.46
1	S_2	3.72	4.20	20	S_2	6.00	7.21
	S_3	5.59	4.57		S_3	8.23	7.57
	S_1	3.40	6.08		S_1	4.20	8.38
5	S_2	4.95	5.82	50	S_2	6.70	8.12
	S_3	7.01	6.19		S_3	9.03	8.49
	S_1	3.64	6.77		S_1	4.44	9.07
10	S_2	5.74	6.51	100	S_2	7.22	8.82
	S_3	7.62	6.88		S_3	9.4	9.18

and the sample intensity λ is defined by the ratio between the number of extreme events and the number of years of observation. Table 1 gives the offshore wave height H_r obtained for each directional sector as function of the relative return period T_r; it is found that the maximum $H_r > 5.0$m is to be found in sector S_3 (the western directions).

In order to test the performance of the system, we thus considered a western storm event with a return period less than 1
5   year, i.e. with significant wave heights that can occur several times a year.
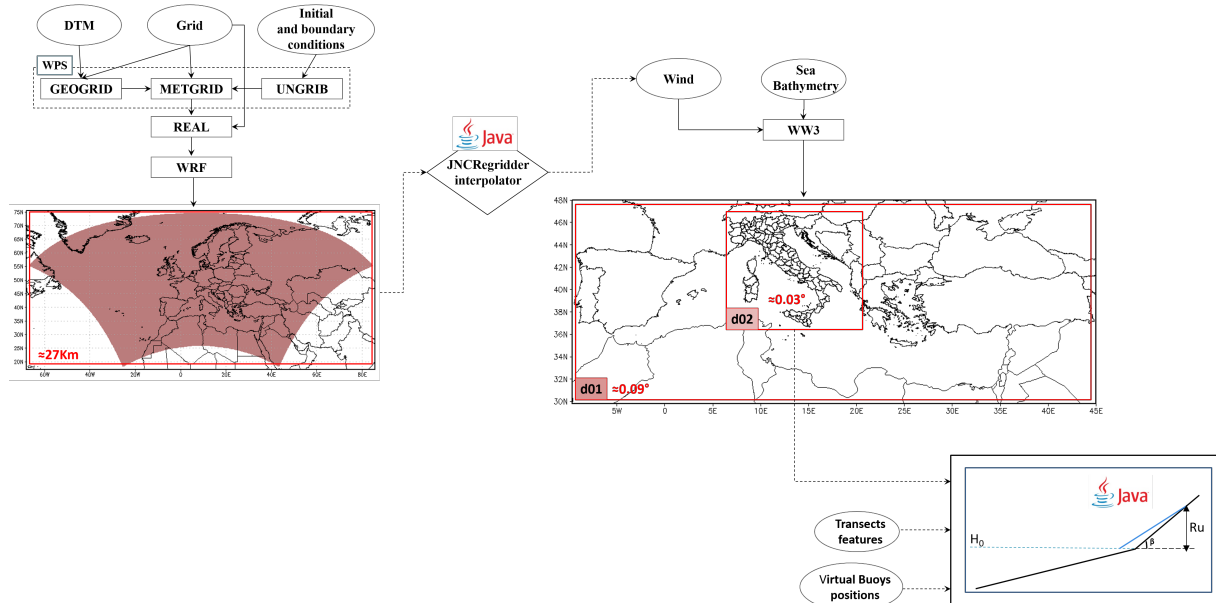
Figure 4. Model chain from the atmospheric model WRF (upper left graphic) to the offshore wave model WW3 (upper right graphic) and the run-up calculator (lower right graphic). The block diagram evidence the input/output components of the model coupling data flux.

3 Methods

3.1 Wave numerical simulations

The weather/sea forecasting tool (Fig. 4) was implemented by CCMMMA using an HPC infrastructure to manage and run a modeling system based on the open-source numerical models Weather Research and Forecasting (WRF) (Skamarock et al.,
5   2001) and WaveWatch III (WW3) (Tolman et al., 2009) organized in a workflow. The operational system is based on complex data acquisition, processing, simulation, post-processing and inter-comparison dataflow, provided by the FACE-IT workflow engine (Pham et al., 2012) which is available as open source and cloud service. This integrated data processing and simulation framework enables: i) the data ingestion from geospatial archives; ii) the data regridding, aggregation, and other processing prior to simulation; iii) the making use of the high-performance and cloud computing; iv) the post-processing to produce
10   aggregated yields and ensemble variables needed for statistics and model testing. The main workflow tool is the WRF numerical model which computes the 10m wind fields and other atmospheric forcing needed to drive the WW3 offshore wave model, which in turn yields the initial and boundary conditions for the shallow water wave simulation of wave transformation and run-up. Wave simulations were carried out using the WW3 model version 3.14, a third generation wave model developed at NOAA/NCEP. The physics packages used in the our implementation are:

15   – Linear input parametrization of Cavaleri and Rizzoli (1981) with a filter for low-frequency energy as introduced by Tolman (1992). Source term package of Tolman and Chalikov (1996) have been implemented with stability correction;

    – Discrete interaction approximation (DIA) (Hasselmann and Hasselmann, 1985) for non-linear wave-wave interactions;

    – ULTIMATE QUICKEST propagation scheme (Leonard, 1979) with averaging technique for Garden Sprinkler alleviation Tolman (2002);

20   – JONSWAP bottom friction formulation (Hasselmann, 1973) with no bottom scattering and Battjes and Janssen (1978) shallow water depth breaking with a Miche-style limiter.

In order to produce the numerical simulations presented in this paper, we configured the WW3 model with two one way nested computational domains:

    – **Coarse domain d01**: it covers almost the whole Mediterranean Sea by a grid of 608x203 points spaced by a 0.09°
25   resolution (Lon_{min}=9.65°W, Lon_{max}=44.98°E; Lat_{min}=29.78°N, Lat_{max}=47.96°N). d01 is thus as a closed domain forced only by the weather conditions provided by the WRF offline coupled data; no wave boundary conditions are therefore to be provided for this domain.

    – **Fine domain d02**: it covers the seas around the Italian peninsula by a grid of 486x353 points spaced by a 0.03° resolution (Lon_{min}=6.33°E, Lon_{max}=20.88°E; Lat_{min}=36.42°N, Lat_{max}=46.98°N). In the used WW3 model configuration, d02 is
30   online coupled with d01 domain.

The outputs from the model include gridded fields with the associated significant wave height (H_s), wave direction (Dir_{mn}), mean period (T_m) and spectral information. The WW3 grid points close to the coast were used as "virtual buoy" (VB) providing the data needed to compute the wave transformation down to the coast, with the final goal of simulating the run-up parameter on the beaches.

3.2 Wave run-up calculator

The last software component of the coupled model chain reported in Fig. 4 (lower right graphic) is the wave run-up calculator on the beach. We used a one-dimensional approach to simulate the beach run-up with a Java software designed to be highly modular as a part of the operational forecasting system. The wave condition in the VB (H_s, T_m and Dir_{mn}) and the beach slope β or β_f derived from a cross-shore beach profile (for example the one shown in Fig. 1), represents the inputs to resolve the run-up empirical equations.

Dealing with random waves, $Ru_{x\%}$ is defined as the wave run-up level, measured vertically from the still water line, which is exceed by $x\%$ of the number of incident waves (van der Meer et al., 2016).

Holman (1986) proposed an empirical formula to obtain $Ru_{2\%}$, based on Iribarren number ξ_f constrained with surf zone slope angle:

$$\frac{Ru_{2\%}}{H_0} = 0.83\xi_f + 0.2 \tag{10}$$

In detail, H_0 is the deep water significant wave height, which can be related to the value at the virtual buoy (VB) through the ratio of the respective wave celerity $C_0 = L_0/T_m$ and $C_{VB} = L_{VB}/T_m$ (Shore Protection Manual, 1984):

$$H_0 = H_s \frac{C_{VB}}{C_0} \tag{11}$$

In VB the wavelength is equal to $L_{VB} = (2\pi)/k$ in which k is the wavenumber obtained by the Hunt approximation of the standard dispersion relation (Fenton and McKee, 1990):

$$(kd)^2 = \left(\frac{\sigma^2 d}{g}\right)^2 + \frac{\left(\frac{\sigma^2 d}{g}\right)}{1 + \sum_{n=1}^{\infty} d_n \left(\frac{\sigma^2 d}{g}\right)^n} \tag{12}$$

where d_n are six constant values given by Fenton and McKee (1990), and σ is the wave frequency.

Mase (1989) on the basis of laboratory tests obtained the characteristic run-up level $Ru_{x\%}$ as a function of two empirical coefficients a and b.

$$\frac{Ru_{x\%}}{H_0} = a\xi^b \tag{13}$$

The Author suggested a=1.86 and b=0.71 for $Ru_{2\%}$, a=2.32 and b=0.77 for Ru_{max}, a=1.70 and b=0.71 for $Ru_{10\%}$, a=1.38 and b=0.70 for $Ru_{33\%}$, a=0.88 and b=0.69 to obtain Ru_{mean}.

9

Stockdon et al. (2006) considered the run-up $Ru_{2\%}$ as a function of two separate terms to consider the different contributions of the wave setup and swash (the latter term on the left hand side)

$$Ru_{2\%} = 1.1 \left(0.35 \tan \beta_f \left(H_0 L_0 \right)^{0.5} + \frac{\left[H_0 L_0 \left(0.563 \tan \beta_f^2 + 0.004 \right) \right]^{0.5}}{2} \right) \tag{14}$$

where β_f is the average slope over a region $\pm 2\sigma$ around $<\eta>$, and σ is the standard deviation of the water level elevation $\eta(t)$. In random waves, H_0 is substituted by the spectral wave height $H_{m0}=4(m_0)^{0.5}$, defined as the incident significant wave height in shallow water, where m_0 is the zero[th] spectral moment.

Poate et al. (2016) proposed the following equation, specifically developed for gravel beaches:

$$Ru_{2\%} = C \tan \beta^{0.5} T_m H_s \tag{15}$$

where C is a constant fixed to 0.49 by the Authors.

The mean beach slope β and the foreshore beach slope β_f, used in the run-up equations are calculated taking into account the examined cross-shore beach profile. The equation (14) has been used by a number of researchers to compute coastal inundation and consequently coastal vulnerability and risk (Di Paola et al., 2014; Benassai et al., 2015a). Melby et al. (2012) compared the skill of some different run-up models through some statistical measures and introduced a new statistical skill measure, described in section 3.3.2, which was used to compare the different formulations for an extensive dataset. In the following, we compared the different run-up equations through the deviation from the observed run-up levels evaluated with video camera records. Among the different empirical formulas used to calculate the wave run-up parameters, the equations (10), (13), (14), (15) have been used to obtain run-up time series. In particular, Holman (1986), Mase (1989), Stockdon et al. (2006) and Poate et al. (2016) formulas have been used for the 2% wave run-up levels, while only Mase (1989) equation has been used to calculate the 10%, 33%, mean and max run-up levels.

3.3 Waves and beach run-up observations

3.3.1 Altimeter and video monitoring

Satellite altimeter data provide a large spatial coverage over the entire region of the Central and Northern Tyrrhenian Sea, which cannot be accomplished by in-situ observations at fixed stations. The offshore part of the model system was therefore validated by making use of remotely sensed data, obtained from the dataset of the Ocean Surface Topography Mission (OSTM/Jason-2), launched on 20 June 2008. Fig. 5 shows the considered track of the OSTM/Jason2 satellite. Geophysical Data Record (GDR) provides ku-based Significant Wave Height data with spatial resolution of 11.2km (Along track) x 5.1km (Across track).

The beach run-up simulations, carried out with the various equations reported above, were validated by means of a video monitoring system placed in the middle of Bonassola beach (Figs. 6a,b,c,d). Video recordings of run-up were made using three video cameras, installed at an elevation of about 13m above Mean Sea Level (MSL), which have allowed a complete coverage of the beach since 19 November 2015 to date. The light intensity of each pixel in the cross-shore transects was digitized by
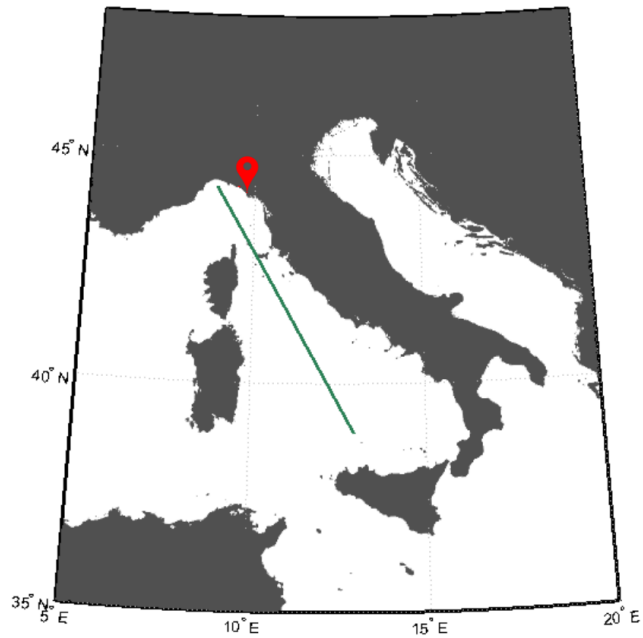
Figure 5. Map showing the WRF and WW3 models spatial domains including the Italian's peninsula overlapped with the location of video-camera system (red marker) and the used OSTM/Jason-2 satellite dataset (green line).
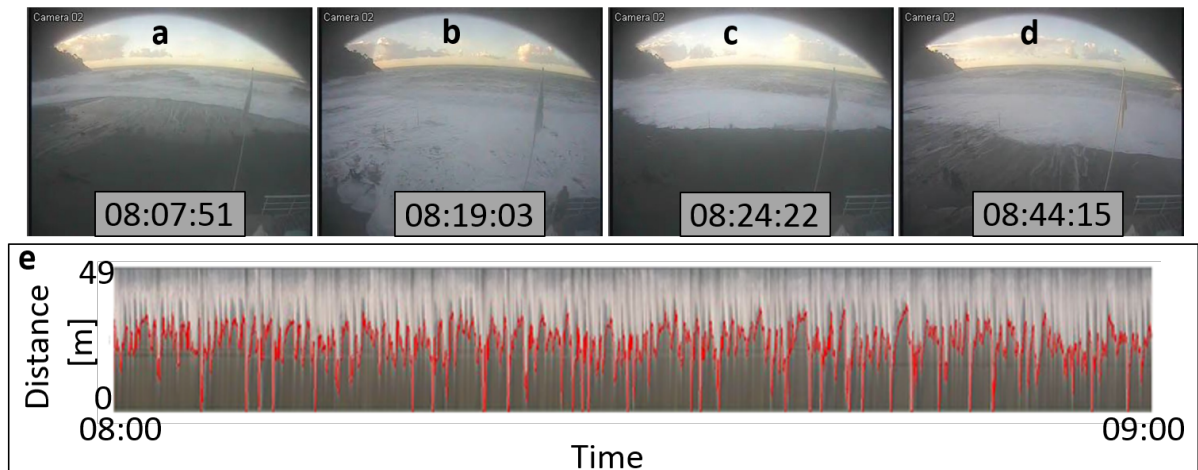
Figure 6. A time sequence (a) (b) (c) (d) of the Bonassola beach sea storm recorded by camera from 08:00 to 09:00 AM on 10 February 2016; (e) timestack obtained by analyzing the videocamera acquisitions in the time interval from 08:00 to 09:00 AM relative to 10 February 2016, highlighting with a red line the detected run-up value.

using the geometric transformation between ground and image coordinates. Vertical run-up elevation time series were extracted from video recordings using the time-stack method (Aagaard and Holm, 1989; Holland and Holman, 1997). This methodology, giving rise to the signal reported in Fig. 6e, is described in the extensive literature on coastal video monitoring (Takewaka and Nakamura, 2001; Ojeda et al., 2008; Zhang and Zhang, 2008). According to Vousdoukas et al. (2012b), the run-up excursion was identified by using the threshold method supplied by Otsu (1975), which is able to identify the wet/dry boundary by pixel colour. The elevation of detected horizontal position (red line in Fig.6e) was calculated using average slope profile obtained from topographic surveys conducted on Bonassola beach. The run-up position at each video sample time (1Hz) was obtained with Beachkeeper plus (Brignone et al., 2012), a software based on Matlab® algorithm used to analyze the images without any a-priory information of the acquisition system. Run-up results have been validated through camera images geo-rectification, which was performed by using 9 Ground control Points (GCPs).The X-Y coordinates of GCPs were acquired in UTM32-WGS84 using DGPS, with 0.15m accuracy on horizontal and vertical positions. The cross-shore resolution of the processed timestack images is 0.2m, equal to the minimum pixel footprint along the monitored transect, in accordance with Vousdoukas et al. (2012a) and Huisman et al. (2011). Best results have been processed with 5 pixel lines analysis, reducing backwash and filtration/extra-filtration detection, using timestack method.

3.3.2 Comparison statistics

The quality of the results provided by the offshore wave model and by the run-up simulations was evaluated by the comparison with wave altimeter records and video-camera run-up observations. Deviation of simulated parameters from observed data was estimated through some of the following statistical error indicators proposed by Mentaschi et al. (2013) (S_i indicate a simulated variable, O_i indicate an observed variable and N is the number of considered observations):

– normalized Bias (BI):

$$BI = \frac{\sum_{i=1}^{N}(S_i - O_i)}{\sum_{i=1}^{N} O_i} \tag{16}$$

– root mean square error (RMSE):

$$RMSE = \sqrt{\frac{\sum_{i=1}^{N}(S_i - O_i)^2}{N}} \tag{17}$$

– normalized root mean square error (NRMSE):

$$NRMSE = \sqrt{\frac{\sum_{i=1}^{N}(S_i - O_i)^2}{\sum_{i=1}^{N} O_i^2}} \tag{18}$$

– normalized scatter index (SI):

$$SI = \sqrt{\frac{\sum_{i=1}^{N}[(S_i - \bar{S}) - (O_i - \bar{O})]^2}{\sum_{i=1}^{N} O_i^2}} \tag{19}$$

– linear correlation coefficient (R):

$$R = \frac{cov(S_i, O_i)}{var(O_i)var(S_i)} \tag{20}$$

The results are summarized in the Summary Performance Score (SPS) index, based on the RMSE, BI and SI performance, normalized between 0 and 1 (as suggested by Melby et al. (2012)).

5

– NRMSE Performance (NRMSE$_P$)

$$NRMSE_P = 1 - NRMSE \tag{21}$$

– BI Performance (BI$_P$)

$$BI_P = 1 - |BI| \tag{22}$$

– SI Performance (SI$_P$)

10

$$SI_P = 1 - SI \tag{23}$$

– Summary Performance Score (SPS)

$$SPS = \frac{NRMSE_P + BI_P + SI_P}{3} \tag{24}$$

4 Experimental results

In this section some experimental results are presented and discussed to show the capability and accuracy of wind-wave

15 modelling chain in estimating run-up levels on the beach studied.

4.1 Offshore wave validation with altimeter data

The consistency of the WW3 model was validated taking full benefit of the altimeter data from OSTM/Jason2 mission, relative to the passage of the satellite during the period from February 9th 2016 at 04:58:44 UTC to 09th 2016 at 05:00:43 UTC. Figs. 7a,b,c depict the simulated WW3 H_s maps on February 10th 2016 at 00:00, 06:00 and 12:00 UTC, with relative zoom, in Figs.

20 7d,e,f, respectively, while Fig. 8 shows the matching between the time history of the measured and modelled offshore H_s along the track.

The results of the wind-wave modelling system were interpolated in both space and time to collocate with the altimeter data. Firstly, hourly WW3 H_s outputs were spatially interpolated (bilinear interpolation) from the grid points to the locations of the altimeter measurements. Interpolations were then carried out in time to fit the satellite pass (linear time interpolation

25 between the previous and following field values). The observed H_s is shown as a blue line in Fig. 8a, while the simulated H_s is reported as a red line. In general, the model fits the measurements quite well, but sometimes it deviates from the observations.

13
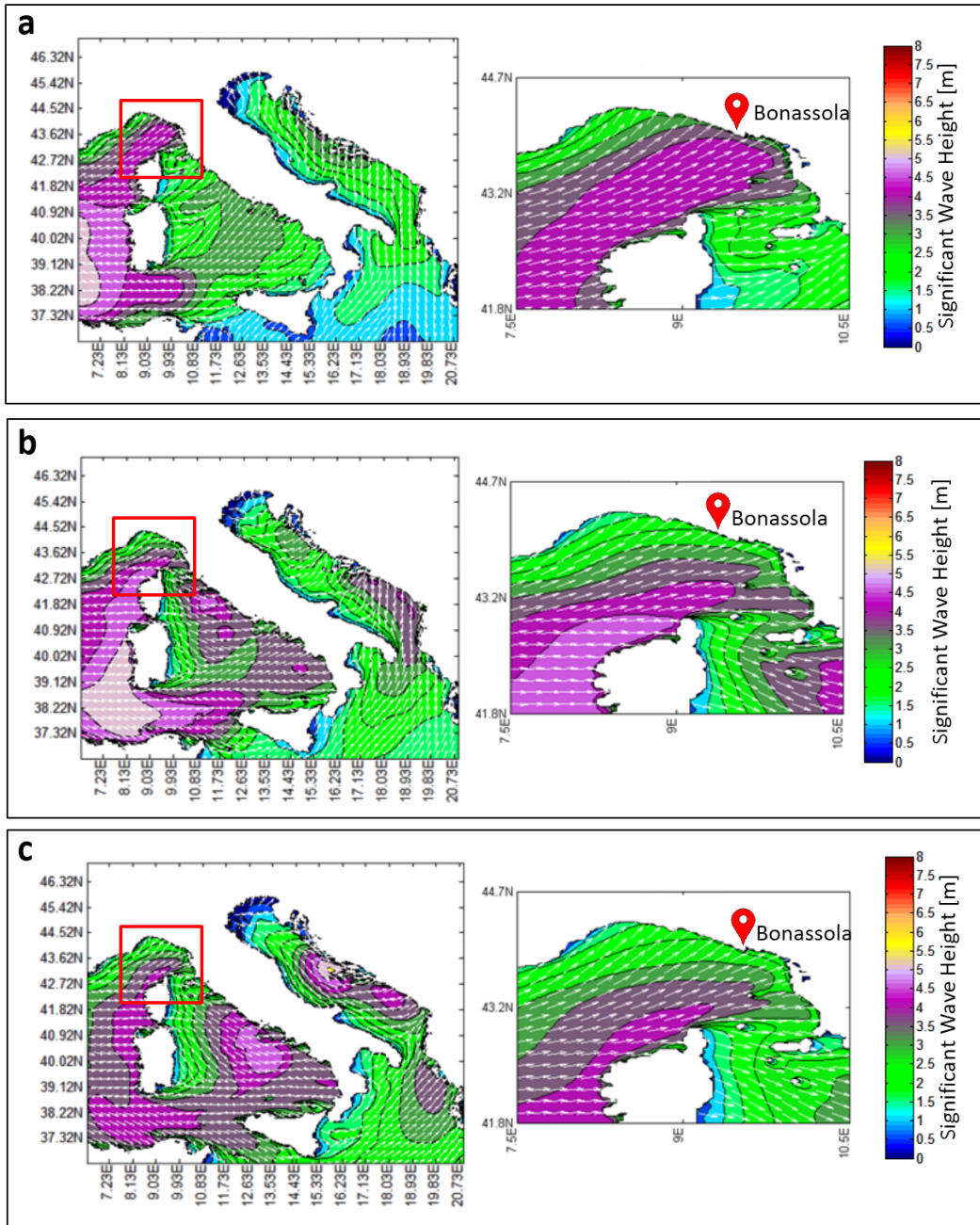
Figure 7. Ligurian Sea significant wave height (color maps) and direction (vector fields) in three moments of sea storm in February 2016. The maps are relative to WW3 model simulation on February 10th 2016 at: (a) 00:00 UTM; (b) 06:00 UTM; (c) 12:00. Wave height isolines are at 0.5m intervals.
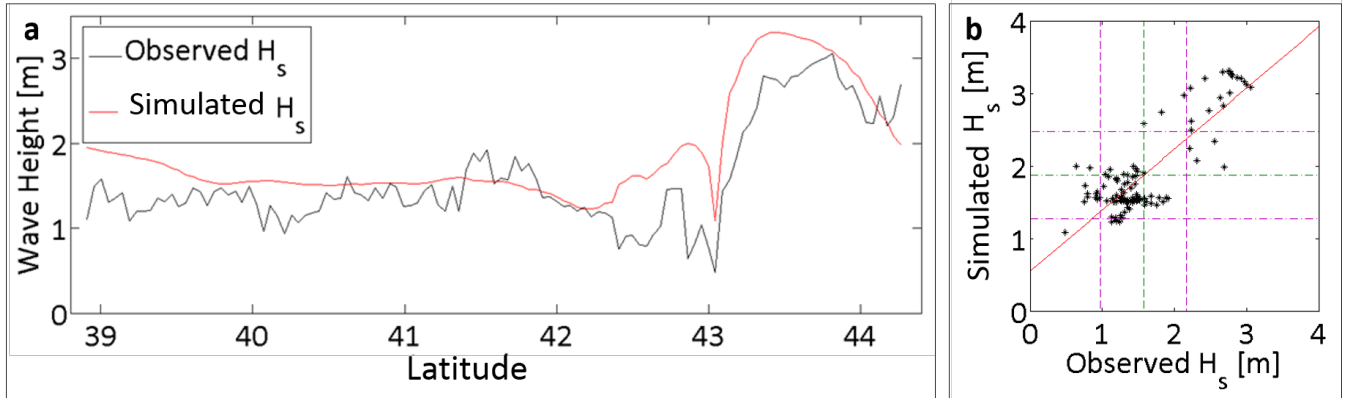
Figure 8. Matching between WW3 and Ku-band altimeter data from JASON-2 satellite pass. 44 cycle 280. (a) Time series during the period from February 9th 2016 at 04:58:44 to 09th 2016 at 05:00:43. (b) Scatter diagram between observed and simulated H_s [m]. The green dotted lines are the mean in x (1.876) and y (1.574) directions, while the purple dotted lines are the relative standard deviation of 0.6022 and 0.5975, respectively.

For example, the first high wave event between 41.5°N and 42°N is underestimated by the model, while the second high wave event between 43.5°N and 44°N is slightly overestimated.

It can also be observed that the simulated H_s trace along the satellite track is much smoother than the observations, due to the fact that the WW3 model is incapable to resolve the small scales seen in the altimeter observations (Reale et al., 2013). The statistics of the comparison give an R value of 0.838, a BI of 0.192, a SI of 0.202 and a RMSE value of 0.455m. The satisfactory agreement is shown by a RMSE lower than 0.46m and by a correlation coefficient higher than 0.83. In fact, Fig. 8 shows a good match between simulations and observations, however non-negligible differences in terms of H_s can be noted, which can be partially explained taking into account the different spatial gridding resolution scale of modeled (WW3) and remotely sensed (Jason-2) wave estimation products.

4.2 Analysis of the existing wave run-up formulas

In Fig. 9 the run-up $Ru_{2\%}$ normalized with H_s has been reported as a function of the Iribarren number for the different equations considered, in a range of the surf similarity parameter corresponding to dissipative and intermediate beaches ($\xi<1.0$). The values of β_f (used in Holman (1986) and Stockdon et al. (2006) equations) has been obtained as a multiple N (fixed to 2.25 for convenience) of β (used in Mase (1989) and Poate et al. (2016) equations). All the equations provide an increase in run-up levels as beaches become more reflective (increase in ξ). In particular, Holman (1986) and Stockdon et al. (2006) equations exhibit a linear increase as a function of ξ, while Mase (1989) and Poate et al. (2016) equations exhibit a nonlinear one.

With regard to the relative run-up levels, Holman (1986) and Mase (1989) equations always represent a higher bound for $Ru_{2\%}$, while Stockdon et al. (2006) equation is a lower bound, at the least for $\xi>0.65$.

Poate et al. (2016) equation is sensitive to H_s: for intermediate storms like the one experienced (H_s=2.5m) it provides low $Ru_{2\%}$

15
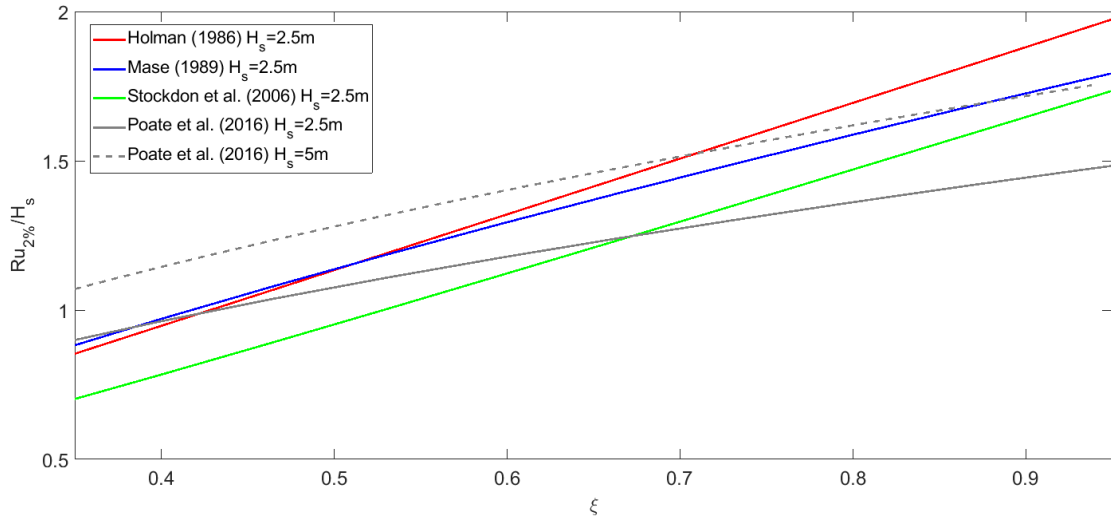
Figure 9. $Ru_{2\%}/H_s$ as a function of Iribarren number ξ for the different equations with reference to the wave conditions of February 2016 storm (H_s=2.5m) and, only for Poate et al. (2016), the same values calculated in more energetic conditions (H_s=5.0m, dotted line)

values, representing a lower bound for ξ>0.65; for severe storms (H_s=5.0m) it gives higher $Ru_{2\%}$ values compared to the other formulas, providing an upper bound for the run-up (dotted line).

4.3 Wave run-up simulations and validation with video-monitoring system

In this subsection, wave run-up numerical simulations obtained with the model chain are described with respect to the storm
5 between February 9th and February 11st 2016. A preliminary offshore wave simulation was performed on a virtual buoy located offshore Bonassola beach. The relative H_s and T_m time history is shown in Figs. 10a,b, respectively. The storm exhibited a maximum H_s higher than 3.0m (with relative T_m of about 7s) on February 10th 2016 at 03:00, followed by a decrease of H_s (with relative increase of T_m) in the following hours, with values between 2.0m and 3.0m, in accordance with the regional wave field maps in Fig. 7.
10 The experimental analysis has been conducted on an average profile, which is provided by beach survey. Since bathymetric and topographic data are subjected to change during storm event, surveys could be repeated after each event to evaluate profile evolution. According to Balduzzi et al. (2014), Bonassola beach is subject to cross-shore sediment movements beyond depth closure and to beach rotation during swell from SE. Therefore, investigated profile has been selected on central area in order to avoid excessive coastline changes.
15 The outcome of run-up assessment showed that the flooding level depends on wave peak period. Despite wave height is almost unchanged, when wave peak period increases of 1.7 seconds,observed wave run-up increase of 0.5 meters and $Ru_{10\%}$ increase from 3.05m to 3.62m, as reported in Fig. 11.

The run-up formulas described in section 3.2 were evaluated considering the wave conditions of February 2016 storm event

and the cross-shore transect reported in Fig. 1c. The simulation results have been compared with the observed wave run-up elevation time series recorded by a beach camera system on February 10th 2016 from 08:00am to 16:00pm. Run-up video records (Fig. 11) were made using the central camera of the video monitoring system described in section 3.3.

The comparison between the different $Ru_{2\%}$ formulas, reported in Fig. 12, shows that the $Ru_{2\%}$ formulas almost always underestimate the levels. In detail, the Holman (1986) results are the highest, followed by Mase (1989), Stockdon et al. (2006) and Poate et al. (2016), in this order. This is consistent with the behaviour of the different formulas evidenced in Fig. 9 for ξ around 0.65, and is confirmed by the RMSE values of 0.41, 0.70, 0.95 and 1.04, respectively, and by the SPS values in decreasing order, 0.92, 0.87, 0.83 and 0.82, respectively (see Fig. 13 and Table 3). The comparison between the hourly mean of the observed and simulated $Ru_{x\%}$, obtained by Mase (1989) equations, reported in Fig. 14, shows more uniform values of the numerical simulations in the eight hours of analysis, due to the lower time resolution of the WW3 model.
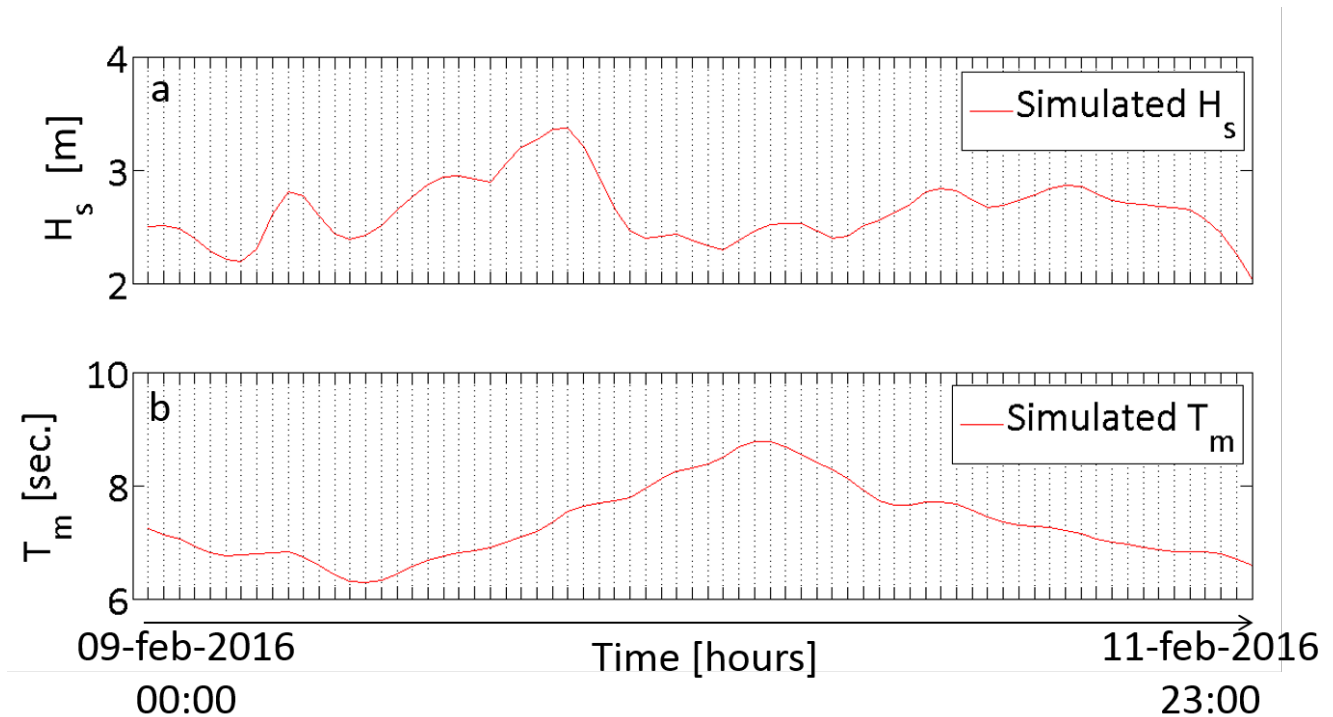
Figure 10. Simulated significant wave height (H_s, figure (a)) and mean wave period (T_m, figure (b)) relative to February 09th-11th 2016 sea storm at virtual buoy near Bonassola beach. The simulations are carried out using WW3 model configured with hourly output timestep.

5   Discussion

In this section, the results of the present study will be discussed, with particular concern to the validation of the offshore and inshore simulations and the operational capability of the modelling chain. The WW3 simulation provided the offshore wave
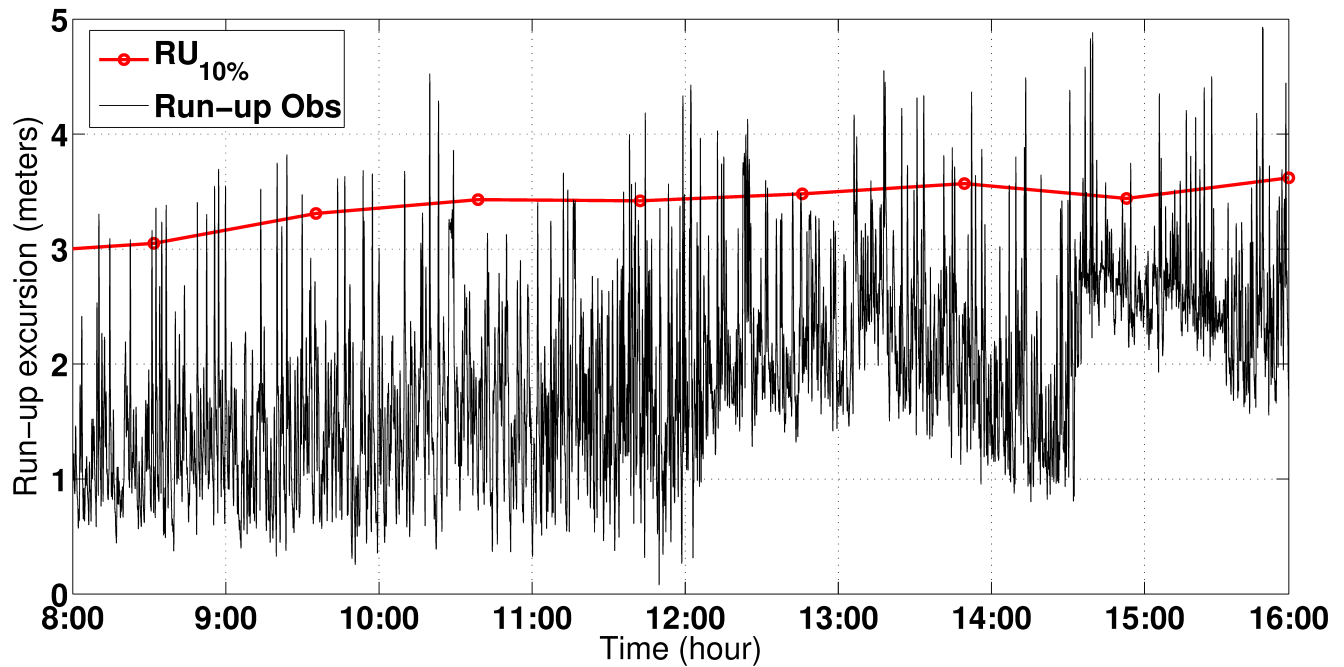
Figure 11. Wave run-up levels collected (black line) using pixel timestacks derived from videocamera data at Bonassola on February 10th 2016 from 8:00 to 16:00 UTC; $Ru_{10\%}$ trend (red line) as obtained by the timestack analysis on 1 hour intervals during investigated time period.
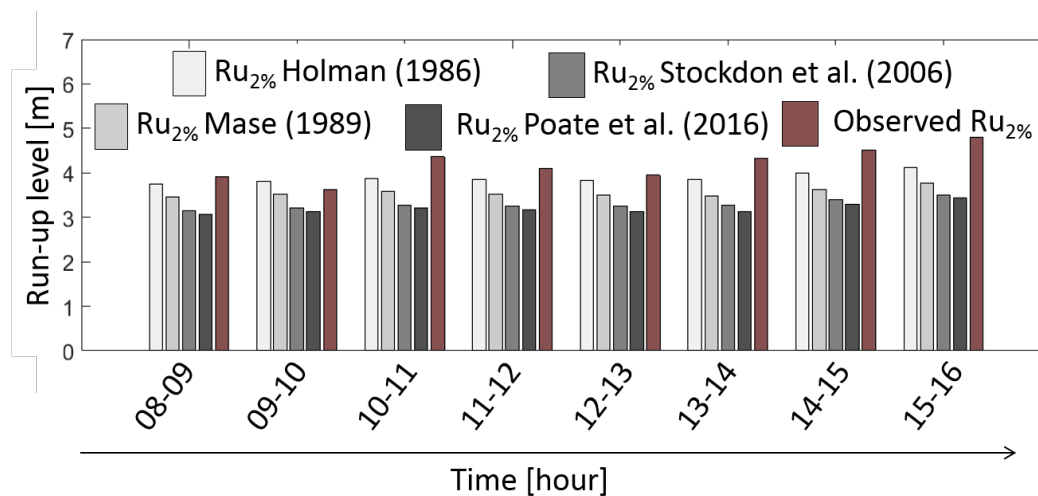

Figure 12. Hourly comparison (February 10th 2016 from 8:00 to 16:00 UTC) among observed and simulated $Ru_{2\%}$. The run-up level simulations are carried out using the empirical formulas introduced by Holman (1986), Mase (1989), Stockdon et al. (2006) and Poate et al. (2016).

Table 2. $Ru_{x\%}$ observed with cameras versus $Ru_{x\%}$ simulated using different equations.

| | Simulated run-up | | | | | | | | | Observed run-up | | | | |
| | Holman (1986) | Mase (1989) | | | | | Stockdon et al. (2006) | Poate et al. (2016) | | | | | | |
	$Ru_{2\%}$	$Ru_{2\%}$	$Ru_{10\%}$	$Ru_{3.3\%}$	Ru_{max}	Ru_{mean}	$Ru_{2\%}$	$Ru_{2\%}$	Ru_{mean}	Ru_{max}	$R_{2\%}$	$R_{10\%}$	$R_{33\%}$
10/02 08-09	3.74	3.46	3.16	2.57	4.22	1.65	3.14	3.07	1.80	4.44	3.92	3.05	2.04
10/02 09-10	3.81	3.52	3.21	2.62	4.30	1.67	3.21	3.13	1.82	3.98	3.63	3.31	2.07
10/02 10-11	3.88	3.58	3.27	2.66	4.38	1.70	3.28	3.21	2.13	4.50	4.36	3.43	2.24
10/02 11-12	3.85	3.53	3.23	2.63	4.33	1.68	3.26	3.17	2.27	4.42	4.10	3.42	2.56
10/02 12-13	3.84	3.49	3.19	2.60	4.29	1.66	3.26	3.13	2.48	4.12	3.95	3.45	2.63
10/02 13-14	3.85	3.48	3.18	2.59	4.28	1.66	3.27	3.13	2.54	4.55	4.33	3.57	2.71
10/02 14-15	4.00	3.63	3.32	2.70	4.46	1.73	3.40	3.29	2.62	4.75	4.52	3.44	2.80
10/02 15-16	4.11	3.76	3.44	2.80	4.62	1.79	3.50	3.44	2.86	5.00	4.80	3.62	2.94

Table 3. Statistical error parameters obtained from the comparison between observed and simulated wave run-up levels.

	R	BI	SI	RMSE	NRMSE	$NRMSE_P$	BI_P	SI_P	SPS
Holman (1986) $Ru_{2\%}$	0.867	-0.075	0.062	0.410	0.097	0.903	0.925	0.938	0.972
Mase (1989) Ru_{mean}	0.424	-0.274	0.157	0.723	0.309	0.691	0.726	0.843	0.753
Mase (1989) $Ru_{33\%}$	0.607	0.059	0.112	0.318	0.126	0.874	0.941	0.888	0.901
Mase (1989) $Ru_{10\%}$	0.576	-0.047	0.039	0.209	0.061	0.939	0.953	0.961	0.951
Mase (1989) $Ru_{2\%}$	0.794	-0.154	0.067	0.704	0.167	0.833	0.846	0.933	0.871
Mase (1989) Ru_{max}	0.763	-0.025	0.051	0.255	0.057	0.943	0.975	0.949	0.956
Stockdon et al. (2006) $Ru_{2\%}$	0.871	-0.217	0.063	0.949	0.225	0.225	0.783	0.775	0.832
Poate et al. (2006) $Ru_{2\%}$	0.845	-0.239	0.063	1.039	0.246	0.754	0.761	0.973	0.817
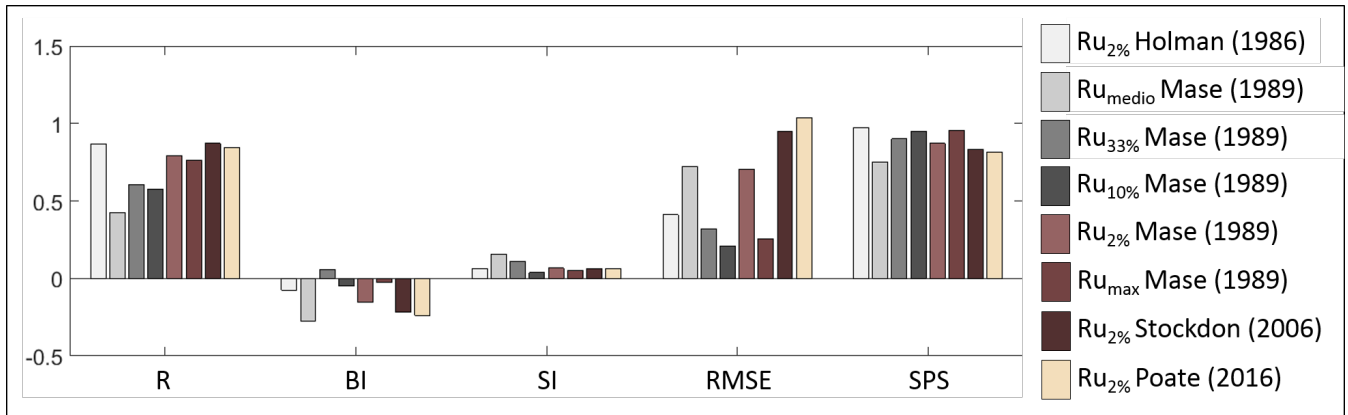
Figure 13. Bar diagram of the statistical parameters R (correlation index), BI (Bias), SI (Scatter Index), RMSE (Root Mean Square Error) and SPS (Summary Performance Score), obtained comparing them run-up video-camera observations with the same parameter calculated using the empirical formulas introduced by Holmann (1986), Mase (1989), Stockdon et al. (2006) and Poate et al. (2016).
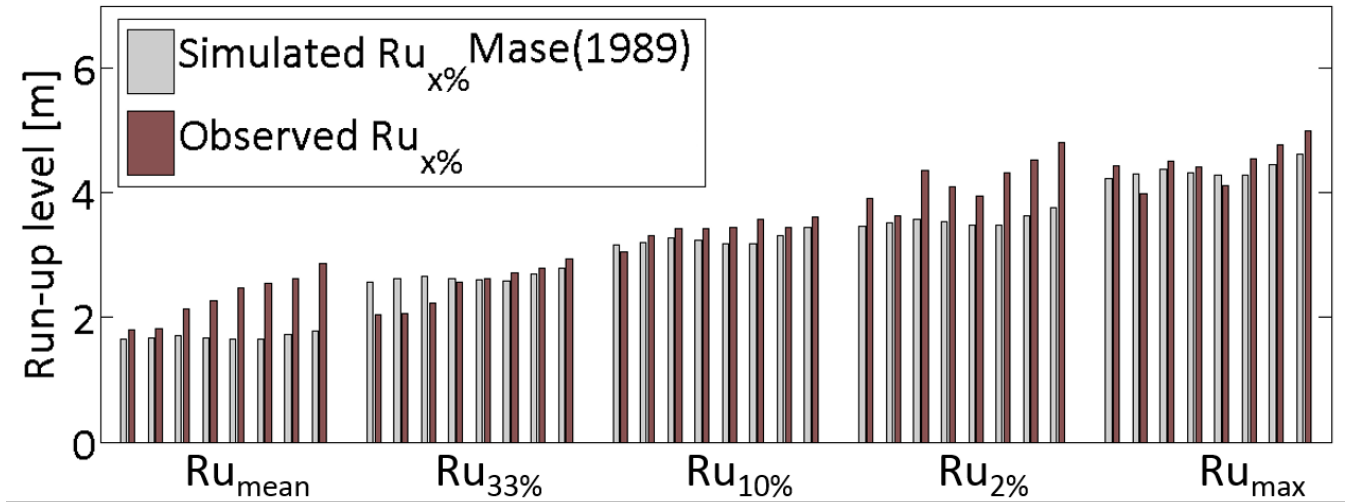
Figure 14. Hourly comparison among different $Ru_{x\%}$ values (Ru_{mean}, $Ru_{33\%}$, $Ru_{10\%}$, $Ru_{2\%}$ and Ru_{max}) calculated with Mase (1989) equations and observations. The run-up data are relative to February 10th 2016 sea storm from 8:00 to 16:00 UTC.

conditions during the examined sea storm, covering the spatial area showed in Fig. 5 (d02 domain). The simulated H_s, sampled along the green track in Fig. 5, were compared with the altimeter one (OSTM/Jason 2 satellite) through a spatial and temporal interpolation which introduced some systematic errors; nevertheless, the validation results of the offshore wave simulations which respect to the altimeter data showed a satisfactory agreement with a BIAS of 0.192 and a standard deviation (SD) lower

5   than 0.6m. These results slightly overpredicted the measured values, in agreement with the ones of Wahle et al. (2017), who compared Saral/Altika altimeter data with the WAM (WAve Model) simulations.

On the other hand, the comparison between the simulated and observed $Ru_{2\%}$ levels on the beach exhibits a general underestimation of the run-up formulas. This discrepancies may be partly given to the limited camera resolution in time stack mode, equal to 0.2 pixel, and to DGPS accuracy of 0.15m. Moreover, additional inaccuracies can be linked to the time shift between

10   model chain output step (1h) and video recording (1s), which produces smoother simulated run-up results, as already evidenced in Fig. 14.

The best matching between simulations and observations is given by the Holman (1986) equation, followed by Mase (1989), Stockdon et al. (2006) and Poate et al. (2016) in this order. This result agrees well with the behaviour of the formulas evidenced in Fig. 9 in the Iribarren range experienced. In particular, this trend is consistent with the behaviour of the Holman (1986) equa-

15   tion, which gives the highest $Ru_{2\%}$ values irrespective of ξ, and with the behaviour of the Poate et al. (2016) equation, which, for the low ξ values experienced, gives a lower bound for $Ru_{2\%}$ for moderate H_s.

The experimental values, in the ξ range considered, are closer to Holman (1986), Mase (1989), Stockdon et al. (2006) and Poate et al. (2016) in this order, in accordance with their RMSE values, which are 0.41, 0.70, 0.95 and 1.04, respectively (see Fig. 13 and Table 3). This is also in agreement with SPS values given in Table 3, and evidences that Stockdon et al. (2006)

20   equation represents a lower bound limit for $Ru_{2\%}$ in the ξ range lower than 0.65. This is consistent with the Poate et al. (2016) considerations, who noted an underestimation of Stockdon et al. (2006) equation, which affected the same Poate et al. (2016) equation for moderate wave conditions. Nevertheless, in more energetic conditions, the Poate et al. (2016) equation represents an upper bound for run-up, at least in the range $\xi>0.65$, as reported in Fig. 9.

25   **6   Conclusions and future directions**

This paper has presented the implementation and the results of a numerical model system aimed at forecasting and/or assessing beach vulnerability starting from input data provided by NOAA GFS global wind and computing the wave run-up over the beach through a chain of offline coupled models. The model chain has been validated with a complex set of experiments carried out on a beach in Northern Italy, aiming at comparing the numerical simulations in both offshore and inshore conditions.

30   The offshore comparison evidenced that the configured wind and wave forecast system provides a satisfactory agreement with the observations, in spite of the limitation due to the relatively low time and space resolution.

The beach run-up comparison evidenced that the Holman (1986) equation appears to be a reliable formula in moderate wave conditions, while Poate et al. (2016) demonstrated that their equation was the best matching one in severe wave conditions,

at least in dissipative beaches. So there is not a universal run-up equation valid for the whole range of sediment grain beach size and wave conditions: this means that a considerable work has still to be done in order to find a general run-up formula for an extended range of wave parameters and beach grain size/slopes. Nevertheless, the comparison between the simulated and observed results shows that the wave run-up simulations obtained by the modelling chain are useful for an alert system, with a

5   proper choice of the run-up equation based on the wave and beach characteristics.

Further improvements of the system will be represented by the enhancement of the model chain resolution thanks to the progresses in cloud computing (Montella et al., 2015) as well as to the GPGPU (General-purpose computing on graphics processing units) based approach (Di Lauro et al., 2012; Montella et al., 2018; Marcellino et al., 2017).

References

Aagaard, T. and Holm, J.: Digitization of wave run-up using video records, Journal of Coastal Research, pp. 547–551, 1989.

Airy, G. B.: Tides and waves, Encyclopaedia Metropolitana, 3, 1817–1845, 1841.

Ascione, I., Giunta, G., Mariani, P., Montella, R., and Riccio, A.: A grid computing based virtual laboratory for environmental simulations,
Euro-Par 2006 Parallel Processing, pp. 1085–1094, 2006.

Aucelli, P. P. C., Di Paola, G., Incontri, P., Rizzo, A., Vilardo, G., Benassai, G., Buonocore, B., and Pappone, G.: Coastal inundation risk
assessment due to subsidence and sea level rise in a Mediterranean alluvial plain (Volturno coastal plain–southern Italy), Estuarine, Coastal
and Shelf Science, 2016.

Aulicino, G., Cotroneo, Y., Ruiz, S., Román, A. S., Pascual, A., Fusco, G., Tintoré, J., and Budillon, G.: Monitoring the Algerian Basin
through glider observations, satellite altimetry and numerical simulations along a SARAL/AltiKa track, Journal of Marine Systems, 179,
55–71, 2018.

Balduzzi, I., Cavallo, C., Corredi, N., and Ferrari, M.: L'érosion des plages de poche de la Ligurie: le cas d'étude de Bonassola (La Spezia,
Italie), Geo-Eco-Trop, 38, 187–198, 2014.

Battjes, J. A.: Surf similarity, in: Coastal Engineering, Proceedings of 14th Conference on Coastal Engineering, Copenhagen, Denmark,
1974, vol. 14, pp. 466–480, ASCE, 1975.

Battjes, J. A. and Janssen, J.: Energy loss and set-up due to breaking of random waves, in: Coastal Engineering 1978, pp. 569–587, 1978.

Benassai, G. and Ascione, I.: Implementation and validation of wave watch III model offshore the coastlines of Southern Italy, in: Proceed-
ings of 25th International Conference on Offshore Mechanics and Arctic Engineering, pp. 553–560, American Society of Mechanical
Engineers, 2006a.

Benassai, G. and Ascione, I.: Implementation of WWIII wave model for the study of risk inundation on the coastlines of Campania, Italy,
Environmental Problems in Coastal Regions VI: Including Oil Spill Studies, 88, 249, 2006b.

Benassai, G., Migliaccio, M., and Montuori, A.: Sea wave numerical simulations with COSMO-SkyMed© SAR data, Journal of Coastal
Research, 65, 660–665, 2013a.

Benassai, G., Montuori, A., Migliaccio, M., and Nunziata, F.: Sea wave modeling with X-band COSMO-SkyMed© SAR-derived wind field
forcing and applications in coastal vulnerability assessment, Ocean Science, 9, 325, 2013b.

Benassai, G., Di Paola, G., and Aucelli, P. P. C.: Coastal risk assessment of a micro-tidal littoral plain in response to sea level rise, Ocean &
Coastal Management, 104, 22–35, 2015a.

Benassai, G., Migliaccio, M., and Nunziata, F.: The use of COSMO-SkyMed© SAR data for coastal management, Journal of Marine Science
and Technology, 20, 542–550, 2015b.

Benassai, G., Di Luccio, D., Corcione, V., Nunziata, F., and Migliaccio, M.: Marine Spatial Planning Using High-Resolution Synthetic
Aperture Radar Measurements, IEEE Journal of Oceanic Engineering, 2018.

Bertotti, L. and Cavaleri, L.: Wind and wave predictions in the Adriatic Sea, Journal of Marine Systems, 78, S227–S234, 2009.

Bidlot, J.-R., Holmes, D. J., Wittmann, P. A., Lalbeharry, R., and Chen, H. S.: Intercomparison of the performance of operational ocean wave
forecasting systems with buoy data, Weather and Forecasting, 17, 287–310, 2002.

Brignone, M., Schiaffino, C. F., Isla, F. I., and Ferrari, M.: A system for beach video-monitoring: Beachkeeper plus, Computers & Geo-
sciences, 49, 53–61, 2012.

Bryan, K. and Coco, G.: Detecting nonlinearity in run-up on a natural beach, Nonlinear Processes in Geophysics, 14, 385, 2007.

Carratelli, E. P., Budillon, G., Dentale, F., Napoli, F., Reale, F., and Spulsi, G.: An experience in monitoring and integrating wind and wave data in the Campania Region, Bollettino di Geofisica Teorica ed Applicata, 48, 215–226, 2007.

Cavaleri, L. and Rizzoli, P. M.: Wind wave prediction in shallow water: Theory and applications, Journal of Geophysical Research: Oceans, 86, 10 961–10 973, 1981.

5 Cotroneo, Y., Aulicino, G., Ruiz, S., Pascual, A., Budillon, G., Fusco, G., and Tintoré, J.: Glider and satellite high resolution monitoring of a mesoscale eddy in the algerian basin: Effects on the mixed layer depth and biochemistry, Journal of Marine Systems, 162, 73–88, 2016.

Dentale, F., Furcolo, P., Pugliese Carratelli, E., Reale, F., Contestabile, P., and Tomasicchio, G. R.: Extreme Wave Analysis by Integrating Model and Wave Buoy Data, Water, 10, 373, 2018.

Di Lauro, R., Giannone, F., Ambrosio, L., and Montella, R.: Virtualizing general purpose GPUs for high performance cloud computing: an 10 application to a fluid simulator, in: Parallel and Distributed Processing with Applications (ISPA), 2012 IEEE 10th International Symposium on, pp. 863–864, IEEE, 2012.

Di Luccio, D., Benassai, G., Di Paola, G., Rosskopf, C., Mucerino, L., Montella, R., and Contestabile, P.: Monitoring and Modelling Coastal Vulnerability and Mitigation Proposal for an Archaeological Site (Kaulonia, Southern Italy), Sustainability, 10, 2017, 2018.

Di Paola, G., Aucelli, P. P. C., Benassai, G., and Rodríguez, G.: Coastal vulnerability to wave storms of Sele littoral plain (southern Italy), 15 Natural hazards, 71, 1795–1819, 2014.

Didenkulova, I.: Marine natural hazards in coastal zone: observations, analysis and modelling (Plinius Medal Lecture), in: EGU General Assembly Conference Abstracts, vol. 12, p. 14748, 2010.

Didenkulova, I. and Pelinovsky, E.: Run-up of long waves on a beach: the influence of the incident wave form, Oceanology, 48, 1–6, 2008.

Didenkulova, I., Sergeeva, A., Pelinovsky, E., and Gurbatov, S.: Statistical estimates of characteristics of long-wave run-up on a beach, 20 Izvestiya, Atmospheric and Oceanic Physics, 46, 530–532, 2010.

Dodd, N.: Numerical model of wave run-up, overtopping, and regeneration, Journal of Waterway, Port, Coastal, and Ocean Engineering, 124, 73–81, 1998.

Doran, K. S., Long, J. W., and Overbeck, J. R.: A method for determining average beach slope and beach slope variability for US sandy coastlines, Tech. rep., US Geological Survey, 2015.

25 Fenton, J. D. and McKee, W.: On calculating the lengths of water waves, Coastal Engineering, 14, 499–513, 1990.

Goda, Y.: On the methodology of selecting design wave height, in: Coastal Engineering Proceedings 1988, vol. 21, pp. 899–913, ASCE, 1989.

Guza, R. and Thornton, E. B.: Swash oscillations on a natural beach, Journal of Geophysical Research: Oceans, 87, 483–491, 1982.

Hasselmann, K.: Measurements of wind wave growth and swell decay during the Joint North Sea Wave Project (JONSWAP), Dtsch. Hydrogr. 30 Z., 8, 95, 1973.

Hasselmann, S. and Hasselmann, K.: Computations and parameterizations of the nonlinear energy transfer in a gravity-wave spectrum. Part I: A new method for efficient computations of the exact nonlinear transfer integral, Journal of Physical Oceanography, 15, 1369–1377, 1985.

Holland, K. T. and Holman, R. A.: The statistical distribution of swash maxima on natural beaches, Journal of Geophysical Research: Oceans, 35 98, 10 271–10 278, 1993.

Holland, K. T. and Holman, R. A.: Video estimation of foreshore topography using trinocular stereo, Journal of Coastal Research, pp. 81–87, 1997.

Holman, R.: Extreme value statistics for wave run-up on a natural beach, Coastal Engineering, 9, 527–544, 1986.

Hubbard, M. E. and Dodd, N.: A 2D numerical model of wave run-up and overtopping, Coastal Engineering, 47, 1–26, 2002.

Huisman, C. E., Bryan, K. R., Coco, G., and Ruessink, B.: The use of video imagery to analyse groundwater and shoreline dynamics on a dissipative beach, Continental shelf research, 31, 1728–1738, 2011.

Hunt, I. A.: Design of sea-walls and breakwaters, Transactions of the American Society of Civil Engineers, 126, 542–570, 1959.

5 Jennings, R. and Shulmeister, J.: A field based classification scheme for gravel beaches, Marine Geology, 186, 211–228, 2002.

Johannessen, O. and Bjorgo, E.: Wind energy mapping of coastal zones by synthetic aperture radar (SAR) for siting potential windmill locations, International Journal of Remote Sensing, 21, 1781–1786, 2000.

Leonard, B. P.: A stable and accurate convective modelling procedure based on quadratic upstream interpolation, Computer methods in applied mechanics and engineering, 19, 59–98, 1979.

10 Marcellino, L., Montella, R., Kosta, S., Galletti, A., Di Luccio, D., Santopietro, V., Ruggieri, M., Lapegna, M., D'Amore, L., and Laccetti, G.: Using GPGPU accelerated interpolation algorithms for marine bathymetry processing with on-premises and cloud based computational resources, in: International Conference on Parallel Processing and Applied Mathematics, pp. 14–24, Springer, 2017.

Mase, H.: Random wave runup height on gentle slope, Journal of Waterway, Port, Coastal, and Ocean Engineering, 115, 649–661, 1989.

Melby, J., Caraballo-Nadal, N., and Kobayashi, N.: Wave runup prediction for flood mapping, Coastal Engineering Proceedings, 1, 79, 2012.

15 Mentaschi, L., Besio, G., Cassola, F., and Mazzino, A.: Developing and validating a forecast/hindcast system for the Mediterranean Sea, Journal of Coastal Research, 65, 1551–1556, 2013.

Montella, R., Giunta, G., and Riccio, A.: Using grid computing based components in on demand environmental data delivery, in: Proceedings of the second workshop on Use of P2P, GRID and agents for the development of content networks, pp. 81–86, ACM, 2007.

Montella, R., Agrillo, G., Mastrangelo, D., and Menna, M.: A globus toolkit 4 based instrument service for environmental data acquisition 20 and distribution, in: Proceedings of the third international workshop on Use of P2P, grid and agents for the development of content networks, pp. 21–28, ACM, 2008.

Montella, R., Giunta, G., Laccetti, G., Lapegna, M., Palmieri, C., Ferraro, C., and Pelliccia, V.: Virtualizing CUDA Enabled GPGPUs on ARM Clusters., in: PPAM (2), pp. 3–14, 2015.

Montella, R., Marcellino, L., Galletti, A., Di Luccio, D., Kosta, S., Laccetti, G., and Giunta, G.: Marine bathymetry processing through 25 GPGPU virtualization in high performance cloud computing, Concurrency and Computation: Practice and Experience, p. e4895, 2018.

Ojeda, E., Ruessink, B., and Guillen, J.: Morphodynamic response of a two-barred beach to a shoreface nourishment, Coastal Engineering, 55, 1185–1196, 2008.

Otsu, N.: A threshold selection method from gray-level histograms, Automatica, 11, 23–27, 1975.

Paprotny, D., Andrzejewski, P., Terefenko, P., and Furmańczyk, K.: Application of empirical wave run-up formulas to the Polish Baltic Sea 30 coast, PloS one, 9, e105 437, 2014.

Pham, Q., Malik, T., Foster, I. T., Di Lauro, R., and Montella, R.: SOLE: Linking Research Papers with Science Objects., in: IPAW, pp. 203–208, Springer, 2012.

Poate, T. G., McCall, R. T., and Masselink, G.: A new parameterisation for runup on gravel beaches, Coastal Engineering, 117, 176–190, 2016.

35 Reale, F., Dentale, F., Carratelli, E. P., and Torrisi, L.: Remote sensing of small-scale storm variations in coastal seas, Journal of Coastal Research, 30, 130–141, 2013.

Reale, F., Dentale, F., Carratelli, E. P., and Torrisi, L.: Remote sensing of small-scale storm variations in coastal seas, Journal of Coastal Research, 30, 130–141, 2014.

Reale, F., Dentale, F., Carratelli, E., and Fenoglio-Marc, L.: Influence of Sea State on Sea Surface Height Oscillation from Doppler Altimeter Measurements in the North Sea, Remote Sensing, 10, 1100, 2018.

Ruggiero, P., Holman, R. A., and Beach, R.: Wave run-up on a high-energy dissipative beach, Journal of Geophysical Research: Oceans, 109, 2004.

5   Rusu, L., Bernardino, M., and Guedes Soares, C.: Wind and wave modelling in the Black Sea, Journal of Operational Oceanography, 7, 5–20, 2014.

Senechal, N., Coco, G., Bryan, K. R., and Holman, R. A.: Wave runup during extreme storm conditions, Journal of Geophysical Research: Oceans, 116, 2011.

Shore Protection Manual, .: Department of the Army, Waterways Experiment Station, Corps of Engineers, Coastal Engineering Researcher

10   Center, 2, 1984.

Skamarock, W. C., Klemp, J. B., and Dudhia, J.: Prototypes for the WRF (Weather Research and Forecasting) model, in: Preprints, Ninth Conf. Mesoscale Processes, J11–J15, Amer. Meteorol. Soc., Fort Lauderdale, FL, 2001.

Stockdon, H. F., Holman, R. A., Howd, P. A., and Sallenger, A. H.: Empirical parameterization of setup, swash, and runup, Coastal engineering, 53, 573–588, 2006.

15   Stockdon, H. F., Sallenger, A. H., Holman, R. A., and Howd, P. A.: A simple model for the spatially-variable coastal response to hurricanes, Marine Geology, 238, 1 – 20, 2007.

Stockdon, K. S. D. H. F., Sopkin, D. S. T. K. S., and Sallenger, N. G. P. A. H.: National assessment of hurricane-induced coastal erosion hazards: Gulf of Mexico, 2012.

Takewaka, S. and Nakamura, T.: Surf zone imaging with a moored video system, in: Proceedings of the International Conference on Coastal

20   Engineering 2000, pp. 1211–1216, ASCE, 2001.

Tolman, H. L.: Effects of numerics on the physics in a third-generation wind-wave model, Journal of physical Oceanography, 22, 1095–1111, 1992.

Tolman, H. L.: Alleviating the garden sprinkler effect in wind wave models, Ocean Modelling, 4, 269–289, 2002.

Tolman, H. L. and Chalikov, D.: Source terms in a third-generation wind wave model, Journal of Physical Oceanography, 26, 2497–2518,

25   1996.

Tolman, H. L. et al.: User manual and system documentation of WAVEWATCH III TM version 3.14, Technical note, MMAB Contribution, 276, 220, 2009.

van der Meer, J., Allsop, N., Bruce, T., De Rouck, J., Kortenhaus, A., Pullen, T., Schüttrumpf, H., Troch, P., and Zanuttigh, B.: EurOtop: Manual on wave overtopping of sea defences and related sturctures-An overtopping manual largely based on European research, but for

30   worlwide application, 2016.

Vousdoukas, M. I., Almeida, L. P. M., and Ferreira, Ó.: Beach erosion and recovery during consecutive storms at a steep-sloping, meso-tidal beach, Earth Surface Processes and Landforms, 37, 583–593, 2012a.

Vousdoukas, M. I., Wziatek, D., and Almeida, L. P.: Coastal vulnerability assessment based on video wave run-up observations at a mesotidal, steep-sloped beach, Ocean Dynamics, 62, 123–137, 2012b.

35   Wahle, K., Staneva, J., Koch, W., Fenoglio-Marc, L., Ho-Hagemann, H. T., and Stanev, E. V.: An atmosphere–wave regional coupled model: improving predictions of wave heights and surface winds in the southern North Sea, Ocean Science, 13, 289, 2017.

Zhang, S. and Zhang, C.: Application of ridgelet transform to wave direction estimation, in: Image and Signal Processing, 2008. CISP'08. Congress on, vol. 2, pp. 690–693, IEEE, 2008.